Gamma motor neurons survive and exacerbate alpha motor neuron degeneration in ALS

Melanie Lalancette-Hebert[a,b], Aarti Sharma[a,b], Alexander K. Lyashchenko[a,b], and Neil A. Shneider[a,b,1]

[a]Center for Motor Neuron Biology and Disease, Columbia University, New York, NY 10032; and [b]Department of Neurology, Columbia University, New York, NY 10032

Edited by Rob Brownstone, University College London, London, United Kingdom, and accepted by Editorial Board Member Fred H. Gage October 27, 2016 (received for review April 4, 2016)

The molecular and cellular basis of selective motor neuron (MN) vulnerability in amyotrophic lateral sclerosis (ALS) is not known. In genetically distinct mouse models of familial ALS expressing mutant superoxide dismutase-1 (SOD1), TAR DNA-binding protein 43 (TDP-43), and fused in sarcoma (FUS), we demonstrate selective degeneration of alpha MNs (α-MNs) and complete sparing of gamma MNs (γ-MNs), which selectively innervate muscle spindles. Resistant γ-MNs are distinct from vulnerable α-MNs in that they lack synaptic contacts from primary afferent (I_A) fibers. Elimination of these synapses protects α-MNs in the SOD1 mutant, implicating this excitatory input in MN degeneration. Moreover, reduced I_A activation by targeted reduction of γ-MNs in $SOD1^{G93A}$ mutants delays symptom onset and prolongs lifespan, demonstrating a pathogenic role of surviving γ-MNs in ALS. This study establishes the resistance of γ-MNs as a general feature of ALS mouse models and demonstrates that synaptic excitation of MNs within a complex circuit is an important determinant of relative vulnerability in ALS.

ALS | motor neuron disease | gamma motor neuron | fusimotor

Amyotrophic lateral sclerosis (ALS) is a fatal disorder characterized by selective motor neuron (MN) degeneration in the brain and spinal cord (1). Not all MN subtypes are equally vulnerable in ALS, and specific subpopulations of MNs, including neurons in the oculomotor and Onuf's nuclei, are preserved even at late stages of disease (2–8). The sparing of these motor pools in ALS is complete, but within the motor pools that are affected the degree to which distinct functional subtypes of MNs are vulnerable varies: fast-fatigable motor neurons are the first to degenerate in ALS patients (9) and in mutant SOD1 mice (10, 11), followed by fatigue-resistant motor units, whereas slow motor units are preserved until late in the course of the disease (12). The reason for the selective vulnerability of distinct subpopulations of MNs in ALS is not known, but factors that determine the unique features of individual MN subtypes, including their size, morphology, and membrane properties, may play a role. In addition, the factors that influence MN vulnerability in ALS may relate to the organization and function of synaptic inputs on each MN subtype that regulate MN activity and control motor output. How the connectivity of MNs within complex motor circuits influences their relative vulnerability in ALS is not known.

Extraocular muscles composed of multiple (fast-, intermediate-, and slow-twitch) fiber types (13) and innervated by ALS-resistant oculomotor neurons are distinct from other skeletal muscles in that no fast, monosynaptic stretch reflex is elicited when these muscles are stretched (14). This observation led us to consider whether the absence of primary sensory inputs might influence the relative vulnerability of other MN subtypes in ALS. We focused on the small γ fusimotor neurons (γ-MNs), which represent approximately one third of all MNs in most limb-innervating motor pools and lack direct excitatory inputs from proprioceptive sensory neurons (5). γ-MNs are distinct from large, force-generating alpha MNs (α-MNs) in that they selectively innervate intrafusal fibers of the muscle spindle and control the sensitivity of spindle afferent discharge (15); beta (β) skeletofusimotor neurons innervate both intra- and extrafusal muscle (16). In addition to morphological differences, distinct muscle targets, and the absence of primary afferent (I_A) inputs on γ-MNs, these functional MN subtypes also differ in their trophic requirements, and γ-MNs express high levels of the glial cell line-derived neurotropic factor (GDNF) receptor Gfrα1 (17). γ-MNs are also molecularly distinguished by the expression of other selective markers including the transcription factor Err3 (18), Wnt7A (19), the serotonin receptor 1d (5-ht1d) (20), and NKAα3 (21). In contrast to α-MNs, γ-MNs also downregulate the expression of the neuronal antigen NeuN and the Hb9::GFP transgene (17, 18).

In several prior studies the absence of selective markers of γ-MN identity and the reliance on size criteria alone made it difficult to assess the role of γ-MNs in ALS patients and in mouse models of disease (22–27). This uncertainty left open several questions about the role of γ-MNs in ALS, including whether a decrease in the average soma size of α-MNs in the disease led to a misidentification of small α-MNs as γ-MNs. Further, if γ-MNs are spared in the SOD1 mouse, what is distinct about γ-MNs that make them less vulnerable, and are they also resistant to degeneration in other models of ALS, thus suggesting common underlying mechanisms of disease? Finally, are there clinical implications of γ-MN survival? Do γ-MNs have a functional role in ALS, either contributing to clinical decline or, alternatively, compensating for α-MN loss in a way that delays onset, slows progression, or increases

Significance

Clinical and pathological hallmarks shared by various familial and sporadic forms of amyotrophic lateral sclerosis (ALS) suggest common underlying mechanisms of disease. Using a series of ALS mouse models, we demonstrate that one shared feature of ALS is the selective sparing of gamma motor neurons (γ-MNs), which innervate muscle spindles and regulate primary proprioceptive afferent (I_A) feedback on alpha motor neurons (α-MNs). Genetic evidence presented here implicates this major excitatory input in the selective degeneration of α-MNs in ALS. Functional elimination of I_A inputs or partial elimination of γ-MNs is protective in superoxide dismutase-1 (SOD1) mutant mice, suggesting that surviving γ-MNs contribute to α-MN loss by increasing muscle afferent-mediated excitation. This study highlights the role of synaptic connectivity and circuit function in motor neuron disease.

Author contributions: M.L.-H. and N.A.S. designed research; M.L.-H. and A.S. performed research; A.S. and A.K.L. contributed new reagents/analytic tools; M.L.-H., A.S., A.K.L., and N.A.S. analyzed data; and A.S. and N.A.S. wrote the paper.

The authors declare no conflict of interest.

This article is a PNAS Direct Submission. R.B. is a Guest Editor invited by the Editorial Board.

Freely available online through the PNAS open access option.

[1]To whom correspondence should be addressed. Email: ns327@columbia.edu.

longevity with the disease? Finally, can fusimotor activity be modified to affect disease?

To address these questions, we used size criteria together with a series of molecular markers to look at γ-MN survival throughout the course of the disease in three transgenic mouse models of ALS: the widely studied $SOD1^{G93A}$ mutant, a line expressing ALS-related human TAR DNA-binding protein 43 (TDP-43; TDP-43^{A315T}), and a recently characterized fused in sarcoma (FUS) mutant expressing human FUS^{P525L} (28). In each of these unrelated models our analysis of MN number and identity revealed complete, selective sparing of γ-MNs in the lumbar spinal cord. As an independent measure of γ-MN survival, we looked at fusimotor inputs to target muscle spindle in the $SOD1^{G93A}$ mutant at the end stage of the disease and found that innervation of intrafusal muscle by γ-MNs is also preserved. These studies provide definitive evidence that γ-MNs are selectively resistant to the toxic mechanisms that cause MN degeneration in ALS and that this resistance is a feature common to various forms of the disease.

To test the idea that excitatory muscle afferent inputs not found on γ-MNs contribute to the selective vulnerability of α-MNs, we took a genetic approach to manipulate elements of the spinal reflex circuit and to remove these synapses functionally in the $SOD1^{G93A}$ mouse. These experiments demonstrate that proprioceptive feedback results in more pronounced MN loss in this ALS mutant and suggest a model in which reflex excitation of α-MNs contributes to their degeneration, accounting in part for their increased vulnerability. Consistent with this model, selective elimination of γ-MNs, which decreases the stretch sensitivity of muscle spindles and the response of I_A afferents, delays the onset and end stage of disease in the $SOD1^{G93A}$ mutant. Our data implicate one major excitatory input in the selective degeneration of MNs and demonstrate that the functional connectivity of MNs within the motor circuit is an important determinant of the differential vulnerability of MNs observed in ALS.

Results

γ-MNs Are Selectively Spared at the End Stage of Disease in the $SOD1^{G93A}$ ALS Mouse. Many studies have shown that in ALS patients and mouse models of disease the average soma size of surviving MNs is significantly reduced. This observation has been interpreted by many to suggest the selective resistance of γ-MNs, whereas others explain the finding as a result of cell shrinkage that precedes cell body loss (22–27, 29). To distinguish between these possibilities, we took advantage of our previous studies in which we identified γ-MNs by the absence of NeuN staining and failure to express the Hb9::GFP transgene (17, 18). We counted MNs at the end stage of disease (at approximately day 150) in $SOD1^{G93A}$ mice and in WT controls. γ-MNs in the WT spinal cord were identified as small choline *O*-acetyltransferase $(ChAT)^+$, $HB9::GFP^-$, $NeuN^-$ cells in the ventral horn (Fig. 1*A*, arrowheads). At end stage, the majority (53%) of $ChAT^+$ MNs at lumbar levels 4 and 5 (L4/5) of the spinal cord had degenerated in the $SOD1^{G93A}$ mutant (243 ± 8 MNs in $SOD1^{G93A}$ mice vs. 512 ± 29 MNs in WT mice; $n = 5$ mice in each genotype; $P = 0.0001$) (Fig. 1*D*), leaving a relative abundance of small, $ChAT^+$, $HB9::GFP^-$, $NeuN^-$ γ-MNs (Fig. 1*B*, arrowheads).

To quantify the relative survival of α-MNs versus γ-MNs throughout the course of disease in the $SOD1^{G93A}$ mice, we used size criteria together with Hb9::GFP and NeuN expression to determine the identity of the remaining $ChAT^+$ L4/5 spinal MNs at various time points. We first observed significant MN degeneration at postnatal day 90 (P90), and this loss progressed throughout life (Fig. 1*D*). At end stage, a size histogram of surviving MNs in the L4/5 spinal cord of mutant and age-matched control mice revealed a dramatic 78% loss of large-diameter (>440 μm^2) $ChAT^+$, $Hb9::GFP^+$, $NeuN^+$ α-MNs in the $SOD1^{G93A}$ mouse compared with WT controls (327 ± 16 MNs in WT vs. 71 ± 5 MNs in $SOD1^{G93A}$ mice; $P < 0.0001$) (Fig. 1*C*, dashed and solid blue lines, respectively, and Fig. 1*D*). In contrast, no significant difference in the number of small-diameter $ChAT^+$, GFP^-, $NeuN^-$ γ-MNs was observed in the $SOD1^{G93A}$ mutant compared with controls (Fig. 1*C*, dashed and solid red lines, respectively, and Fig. 1*D*), demonstrating the selective sparing of this subpopulation of fusimotor neurons.

As further evidence of the fusimotor identity of these surviving MNs, we looked at the expression of the GDNF receptor Gfrα1, one of several molecular markers recently reported to distinguish postnatal α-MNs and γ-MNs (17, 19). γ-MNs are selectively dependent on GDNF signaling in the embryo (30) and on muscle spindle-derived GDNF in the postnatal period (17). Consistent with this trophic dependence, mature γ-MNs express a relatively high level of Gfrα1 compared with α-MNs, as shown by the $Gfrα1^{TLZ}$ reporter mice (17). Analysis of the $SOD1^{G93A}$ mice at disease end stage revealed that surviving MNs in the L5 ventral horn express a high level of the Gfrα1 reporter (Fig. 1*E*, arrowheads) compared with large-diameter $ChAT^+$ cells (Fig. 1*E*, asterisks). Moreover, the number of $Gfrα1^{TLZ+}$ cells was comparable in the mutant and control groups both early in the course the disease (P90) and at end stage (Fig. 1*F*), providing further evidence that γ-MNs are selectively spared in the $SOD1^{G93A}$ mutants.

Fusimotor Innervation of Intrafusal Muscle Fibers Is Preserved at End Stage in $SOD1^{G93A}$ Mice. Our analysis of γ-MN somata demonstrated that fusimotor neurons are spared in the $SOD1^{G93A}$ mouse; however one cannot conclude from the persistence of γ-MN cell bodies that connections to muscle spindles are also preserved. To address this question and provide further evidence of γ-MN sparing in this model of ALS, we examined extra- and intrafusal neuromuscular junctions (NMJs) in the $SOD1^{G93A}$ mouse to determine the extent of fusimotor denervation. Approximately 90% of fusimotor axons innervating intrafusal muscle derive from $Hb9::GFP^-$ γ-MNs; the remainder are β-skeletofusimotor collaterals of $Hb9::GFP^+$ α-MNs (17). Therefore, selective preservation of γ-MNs in this mutant would predict only minimal denervation of intrafusal fibers at the end stage of disease. In $SOD1^{G93A}$ mice we used fluorescent α-bungarotoxin to visualize the intrafusal NMJ and antibodies against protein gene product 9.5 (PGP9.5) (17) to label the annulospiral primary sensory endings and motor axons in the tibialis anterior (TA) muscle (Fig. 2 *A–D*), a largely fast-twitch muscle innervated by a relatively vulnerable population of α-MNs from the L4 and L5 spinal cord (11). PGP9.5 is also weakly expressed in intrafusal muscle fibers, making it possible to identify intrafusal motor endings in the juxtaequatorial and polar regions of the muscle spindle. In agreement with previous reports (10), we found that the majority (66 ± 6.3%; $n = 555$ NMJs; $P < 0.0001$) of NMJs in the extrafusal fibers of the TA muscle are vacant at P150 in the $SOD1^{G93A}$ mice (Fig. 2 *C* and *E*). In contrast, the great majority (92 ± 3.5%, $n = 25$ spindles; $P = 0.08$) of the intrafusal NMJs in the $SOD1^{G93A}$ mouse remained innervated (Fig. 2 *D* and *E*), correlating precisely with the percentage of fusimotor (91%) versus skeletofusimotor (9%) inputs in TA muscle spindles (17). These data are consistent with the selective loss of β collaterals of α-MNs and the preservation γ-fusimotor inputs even at the end stage of disease in mutant $SOD1^{G93A}$ mice.

The Resistance of γ-MNs Is a Common Feature of SOD1, TDP-43, and FUS Mouse Models of ALS. To determine whether the resistance of γ-MNs in $SOD1^{G93A}$ mice is also observed in other models of familial ALS, we used the same methods to quantify MN loss in two unrelated transgenic models ALS, one in which mutant human

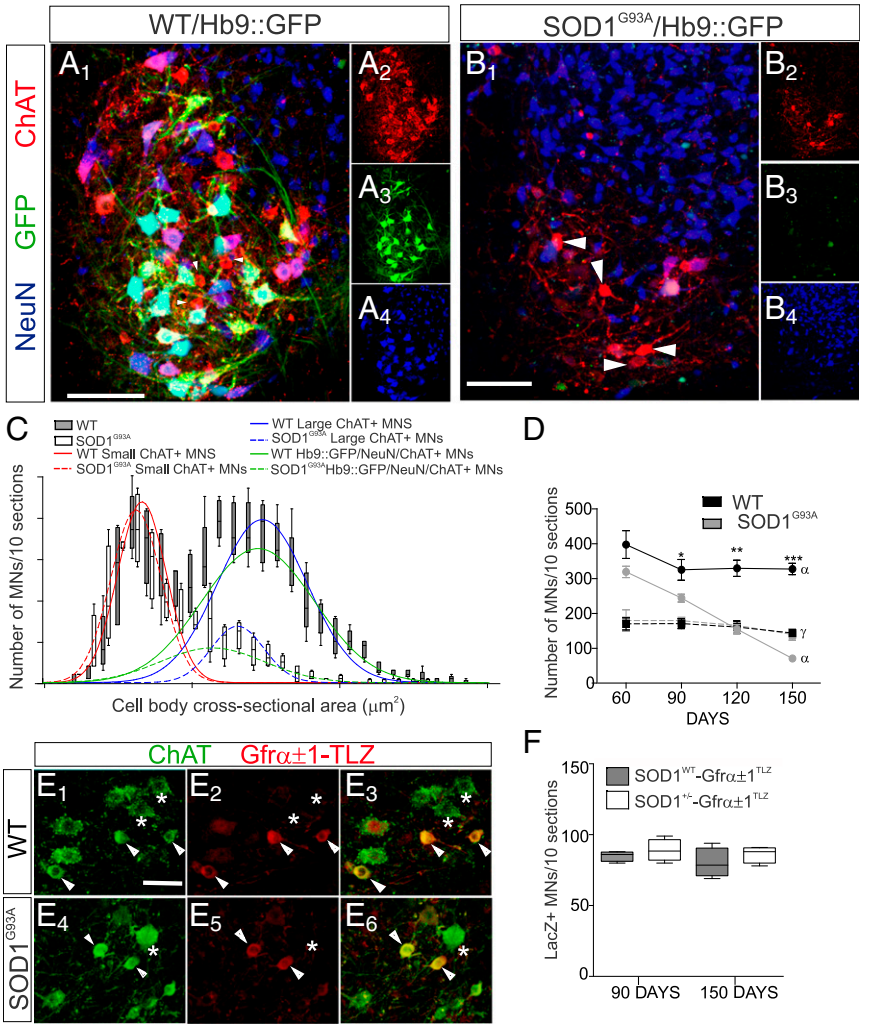

Fig. 1. Small γ fusimotor neurons are selectively spared at the end stage of disease in SOD1^{G93A} mice. (*A* and *B*) MNs in the L5 segment of WT (*A*) and SOD1^{G93A} (*B*) animals at the end stage of disease (~ day 150). Animals are heterozygous for the Hb9::GFP transgene in which GFP is selectively expressed in large α-MNs. (*A*) α-MNs thus are identified by positive immunoreactivity for ChAT (red), GFP (green), and NeuN (blue), and γ-MNs are identified by positive immunoreactivity for ChAT and negative immunoreactivity for NeuN and GFP. (*B*) γ-MNs (arrowheads) are preserved in SOD1^{G93A} animals at end stage. (Scale bars: 200 μm.) (*C*) Size distribution of all ChAT$^+$ MNs in WT (gray bars; 50-μm^2 bins; $n = 5$ mice) and SOD1^{G93A} animals (white bars, $n = 5$ mice). ChAT$^+$ MN cell body sizes showed a bimodal distribution best fit by two Gaussian curves (correlation = 0.93) representing small WT (solid red line) and small SOD1 (dashed red line) and large WT (solid blue line) and large SOD1 (dashed blue line) populations. These measurements were used to determine the cutoff of the small ChAT$^+$ γ-MNs. In WT animals, the small-size ChAT$^+$ population had a mean cross-sectional area (± SD) of 310 ± 67 μm^2. The large population had a wider distribution with a mean cross-sectional area of 687 ± 211 μm^2. The size cutoff distinguishing small and large ChAT$^+$ MNs was 440 μm^2. Small MNs represent 36.2 ± 1.7% of the total ChAT$^+$ MNs. In the SOD1^{G93A} mice, the small ChAT$^+$ MNs had a mean cross-sectional area (± SD) of 300 ± 96 μm^2, and the large ChAT$^+$ MNs had a mean cross-sectional area (± SD) of 526 ± 238 μm^2. The subpopulation of ChAT$^+$ α-MNs (HB9::GFP/NeuN$^+$) is represented by two different Gaussian curves: WT, 715 ± 186 μm^2, correlation 0.76 (solid green line), and SOD1^{G93A}, 563 ± 173 μm^2, correlation 0.80 (dashed green line). Error bars represent the 95% confidence interval. (*D*) Quantification of α-MNs and γ-MNs in the L4/L5 segment of the spinal cord. At end stage (day 150), there is a significant (78%, $^{***}P < 0.0001$) loss of the large-size α-MN population in animals carrying the SOD1^{G93A} transgene as compared with WT controls. No significant difference is observed in the small-sized Hb9::GFP$^-$, NeuN$^-$ γ-MN population. The loss of α-MNs becomes significant at day 90 (60 d: $P = 0.26$; 90 d: $^*P = 0.0267$; 120 d: $^{**}P = 0.0009$). (*E*) MNs in the L5 segment of end-stage WT (E_1–E_3) and SOD1^{G93A} (E_4–E_6) animals demonstrate that small-sized ChAT$^+$ cells (white arrowheads) express high levels of the Gfrα1-TLZ compared with large-sized ChAT$^+$ MNs (white asterisks). (Scale bar: 100 μm.) (*F*) There is no significant difference in the number of Gfrα1^{TLZ+} MNs in SOD1^{G93A} (gray) and WT (white) animals at P90 and at end stage (~P150). Error bars represent the 95% confidence interval.

TDP-43 is expressed under the control of the Prp promoter (Prp-TDP-43^{A315T}) (31, 32), and another in which ALS mutant human FUS (hFUS^{P525L}) is expressed from the mouse *MAPT* tau (τ) locus (τ^{ON}hFUS^{P525L}) (28).

Previous analysis of the TDP-43^{A315T} mouse showed ~20% reduction in MNs in the L3–L5 spinal cord (32). Our analysis revealed that small ChAT$^+$, GFP$^-$, NeuN$^-$ cells were still present at the end stage of disease (around P165) in this mutant, and size histograms demonstrate distinct γ-MN and α-MN populations (Fig. 3 *A*–*C*). Using a cutoff of 465 μm^2 as the upper limit of the small-diameter γ-MNs, we observed a reduction of ~18% in the total number of L5 MNs (510 ± 24 MNs in WT mice, $n = 7$ mice versus 416 ± 25 MNs in TDP-43^{A315T} mice, $n = 5$ mice; $P = 0.02$) (*Experimental Procedures*), which could be accounted for entirely by a 27.5% reduction in the number α-MNs (339 ± 17 α-MNs in WT mice versus 246 ± 9 α-MNs in TDP-43^{A315T} mice). Again, no difference in the total number of γ-MNs (ChAT$^+$, NeuN−, and size <465 μm^2) was observed (Fig. 3*D*), demonstrating the resistance of fusimotor neurons to the toxic effects of the ALS-causing mutant TDP-43 as well as to SOD1.

To determine if this same subtype selectivity also characterized MN degeneration in the FUS-mutant mice, we measured the size of surviving L5 MNs at P360. Using similar size criteria and NeuN staining as markers of α-MN versus γ-MN identity, this analysis also revealed a complete sparing of γ-MNs despite the expression of ALS mutant myc-hFUS in this MN subpopulation (Fig. 3*F*). At this time point more than 40% of large NeuN$^+$ α-MNs ($P \leq 0.001\%$) (Fig. 3 *E* and *G*), corresponding to ~30% of all L5 MNs (Fig. 3 *E* and *G*), are lost in the τ^{ON}hFUS^{P525L} mutant (28), but the number of γ-MNs in the mutant animals versus age-matched control animals was unchanged ($P > 0.05\%$) (Fig. 3 *E* and *G*). Together, these data demonstrate that the resistance of γ-MNs is a common feature of disease across distinct models of ALS and suggest shared pathogenic mechanisms in various forms of familial ALS.

The Effect of Excitatory Sensory Inputs on MN Survival in SOD1^{G93A} Mutant Mice. The resistance of γ-MNs in these three mouse models led us to consider the properties of γ-MNs that distinguish them from α-MNs and that may underlie their resistance to the toxic effects of mutant SOD1, TDP-43, and FUS. γ-MNs are found within the same motor pools and are subject to the same local influences as vulnerable α-MNs, but some aspect of their phenotype is protective. The mechanisms that lead to the

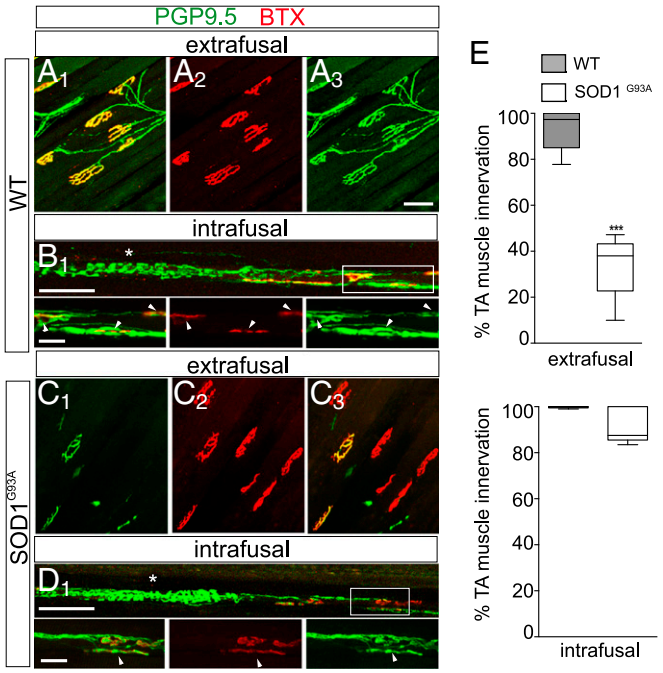

Fig. 2. Innervation of intrafusal muscle fibers is preserved in end-stage SOD1^{G93A} mice. (*A–D*) Representative images of the TA muscle from WT (*A* and *B*) and SOD1^{G93A} (*C* and *D*) animals showing NMJs on extrafusal (*A* and *C*) and intrafusal (*B* and *D*) muscle fibers. Innervation of muscle was determined by colocalization of markers for motor axon terminals (anti-PGP 9.5 antibody) and the acetylcholine receptors of the postsynaptic surface of the NMJ (fluorophore-conjugated α-BTX). Marked denervation of extrafusal NMJs is observed in the SOD1^{G93A} mouse at end stage (*C*). Annulospiral primary sensory endings (asterisk in *B1* and *D1*), motor axons in intrafusal fibers, and intrafusal muscle also show immunoreactivity for PGP 9.5, allowing identification of the intrafusal motor endings in the juxtaequatorial and polar regions of the muscle spindle. In both WT (*B1*) and SOD1^{G93A} (*D1*) animals, intrafusal NMJs are innervated by PGP9.5^{+} motor axons (arrowheads). (Scale bars: 50 μm.) (*E*, *Upper*) The majority (66 ± 6.3%; ***$P <$ 0.0001) of NMJs in the extrafusal fibers of the TA are vacant at P150 in the SOD1G93A mice. (*Lower*) The great majority (92 ± 3.5%) of the intrafusal NMJs remained innervated. The limited amount of denervation presumably is caused by the selective loss of the fusimotor collaterals of β-MNs. Error bars represent the 95% confidence interval.

differentiation of γ-MNs from α-MNs have not been elucidated, although molecular differences have been described (5). Intrinsic (molecular) differences may account for the selective vulnerability of α-MNs versus γ-MNs in ALS, but other distinctions between these MN subtypes may play a role also. For example, unlike α-MNs, γ-MNs do not receive monosynaptic excitatory inputs from I_A proprioceptive afferents; in this way, γ-MNs are like oculomotor neurons, another population of MNs selectively spared in ALS (33, 34). Moreover, MNs in Onuf's nucleus that control defecation, micturition, and ejaculation are also preserved in ALS (35), and, as is consistent with excitatory proprioceptive inputs having a role in MN degeneration in ALS, these MNs do not receive vesicular glutamate transporter 1 (VGluT1) inputs, as shown in a caudal (L6) lumbar section of the mouse spinal cord (Fig. 4*I*). This correlation suggests that excitatory proprioceptive innervation may contribute to MN loss in ALS.

To test the possibility that muscle-afferent activity plays a role in α-MN degeneration, we examined the effect of SOD1^{G93A} in the early growth response factor 3 (Egr3) mutant (Egr3^{KO}) mice in which muscle spindles degenerate (36), resulting in a profound functional deficit in the strength of direct (I_A) sensory–motor connections (Fig. 4*A*) (37). Comparison of SOD1^{G93A}/Egr3^{KO} double-mutant mice and controls revealed no effect on the lifespan of the SOD1^{G93A} mutants (median survival: 159 d for Egr3^{WT}-SOD1^{G93A} mice and versus 157 d for Egr3^{KO}/SOD1^{G93A} mice; $P = 0.67$) (Fig. 4*B*). Nonetheless, Egr3 deficiency did appear to have a protective effect in the SOD1^{G93A} mutant mice in terms of α-MN survival. γ-MN loss caused by the elimination of Egr3 (17, 36) combined with α-MN loss in the SOD1^{G93A} mutant resulted, not surprisingly, in a greater overall reduction in the total number of L4/5 spinal MNs at end stage (~P157) in the SOD1^{G93A}/Egr3^{KO} double mutants (138 ± 8 MNs) compared with WT mice (455 ± 38 MNs), SOD1^{G93A} single mutants (198 ± 12 MNs), and Egr3^{KO} controls (384 ± 78 MNs). Consistent with our finding of γ-MN sparing in the SOD1^{G93A} mouse, size distribution analysis revealed no significant difference in the total number of γ-MNs in the Egr3^{KO} versus SOD1^{G93A}/Egr3^{KO} double-mutant animals. However, we saw significantly ($P = 0.04$) less α-MN loss in the SOD1^{G93A}/Egr3^{KO} double mutant than in the SOD1^{G93A} control (89 ± 7 surviving α-MNs in the SOD1^{G93A}/Egr3^{KO} double mutant vs. 54 ± 8 surviving α-MNs in the SOD1^{G93A} single mutant) (Fig. 4*C*), demonstrating that functional elimination of muscle spindle afferents had a protective effect on α-MNs in the context of ALS mutant SOD1.

Further evidence of this protective effect came from an analysis of NMJs in the relatively vulnerable TA muscle, where one would expect the effects of Egr3 deficiency on the SOD1^{G93A} MN phenotype to be most pronounced. Although 74% ± 2.8% of extrafusal NMJs were denervated in the TA muscle in the Egr3^{WT}-SOD1^{G93A} mouse, only 60% ± 3% of NMJs in the Egr3^{KO}-SOD1^{G93A} double mutant had no associated motor axon ($P = 0.02$) (Fig. 4*D*), demonstrating that the loss of excitatory I_A afferent inputs on α-MNs results in a significant (~20%) reduction in muscle denervation in the SOD1^{G93A} ALS mouse.

A Functional Role for γ-MNs in Regulating α-MN Loss in SOD1^{G93A} Mice. Our findings of reduced α-MN loss and extrafusal muscle denervation in the Egr3^{KO}/SOD1^{G93A} double mutant suggests a model in which proprioceptive sensory activity contributes to α-MN degeneration in ALS and the absence of I_A afferents on γ-MNs accounts, at least in part, for their selective survival. However, this interpretation of the Egr3^{KO} phenotype is potentially complicated by the fact that muscle spindle degeneration results not only in the degeneration of muscle spindles and the consequent functional loss sensory–motor connections (37, 38) but also in the selective degeneration of γ-MNs (36), possibly confounding our analysis of the muscle spindle mutants. Given that the primary role of γ-MNs is to regulate the sensitivity of muscle spindles and the firing rate of I_A afferents in response to stretch (39), our model would predict that loss of γ-MNs would have a protective effect in the SOD1^{G93A} mouse by reducing proprioceptive feedback on α-MNs. However, the loss of fusimotor activity in the context of this ALS model has not been tested. Therefore we considered whether γ-MN elimination has any effect on α-MN degeneration or other aspects of the SOD1^{G93A} phenotype that might suggest a functional and possibly clinically significant role of surviving γ-MNs in ALS.

To explore the role of fusimotor activity in the onset and progression of the MN phenotype in the SOD1^{G93A} mouse, we used an approach we characterized previously to eliminate γ-MNs in the SOD1^{G93A} mouse selectively by knocking out muscle spindle-derived GDNF on which postnatal γ-MN survival depends (17). We did so using a floxed allele of GDNF and a muscle spindle-specific Cre deleter strain, Egr3-IRES-Cre (Egr3-CRE). In mice double homozygous for these two alleles (GDNF$^{FLOX/FLOX}$;Egr3$^{CRE/CRE}$, henceforth referred to as "GDNF^{FLOX}/Egr3^{CRE}"), we investigated whether the elimination of fusimotor neurons had any effect on α-MN survival, disease onset, or lifespan in the SOD1^{G93A} mutant. Our previous analysis of the GDNF^{FLOX}/Egr3^{CRE}

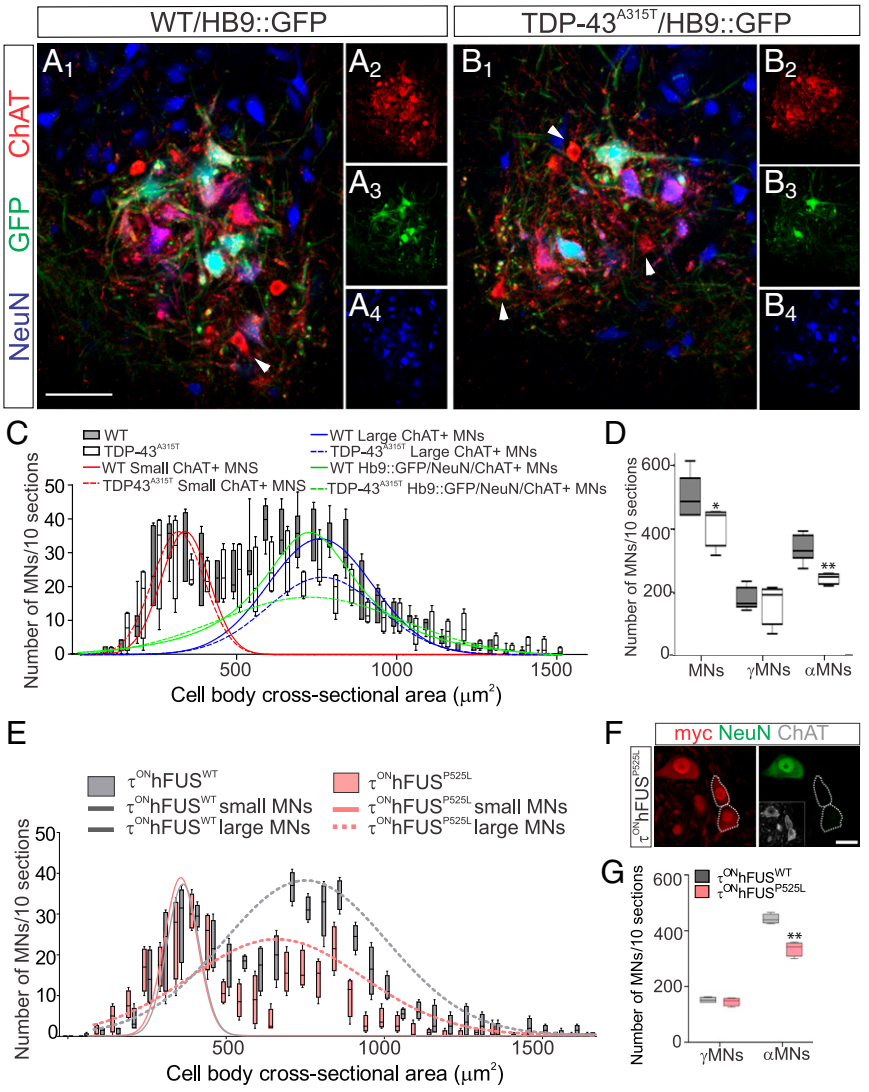

Fig. 3. Gamma fusimotor neurons are also spared in the TDP-43^{A315T} and hFUS^{P525L} mutants. Shown is the shared selectivity of MN degeneration across different models of familial ALS. (*A* and *B*) Representative images of the L5 segment from WT (*A*) and TDP-43^{A315T} (*B*) mice at the end stage of disease (~P150) showing immunoreactivity for ChAT (A_2 and B_2, red), GFP (A_3 and B_3, green), and NeuN (A_4 and B_4, blue). Small-sized ChAT$^+$, GFP$^-$, NeuN$^-$ γ-MNs (white arrowheads in *A* and *B*) are preserved in the ventral horn of the spinal cord of the TDP-43^{A315T} mice at end stage. (Scale bar: 100 μm.) (*C*) Bimodal distribution of cell-body size of all ChAT$^+$ MNs in WT mice (gray bars; 50-μm^2 bins; $n = 7$) and TDP-43^{A315T} mice (white bars; $n = 7$) fit by two Gaussian curves (correlation = 0.71) representing small WT (solid red line) and TDP43 (dashed red line) and large WT (solid blue line) and TDP-43 (dashed blue line) populations. In the WT mice, the small ChAT$^+$ MNs had a mean (± SD) cross-sectional area of 318 ± 75 μm^2. Large ChAT$^+$ MNs showed a wider size distribution around a mean (± SD) of 688 ± 204 μm^2. We used an area of 465 μm^2 as the cutoff point to distinguish between small and large MNs. In the TDP43^{A315T} mice, the small-sized ChAT$^+$ population had a mean cross-sectional area (± SD) of 311 ± 77 μm^2, and the large-size MNs had a mean area (± SD) 652 ± 271 μm^2. All α-MNs (Hb9::GFP/NeuN$^+$) are represented by two different Gaussian curves: WT (green solid line): 718 ± 180 μm^2, correlation 0.70, and TDP-43^{A315T} (green dashed line): 724 ± 289 μm^2, correlation 0.72. Error bars represent the 95% confidence interval. (*D*) Quantification of ChAT$^+$ MNs shows an 18.6% reduction (*$P = 0.02$) in in the total number of L5 MNs [WT (gray): 510 ± 24 MNs; TDP-43^{A315T} (white): MNs 416 ± 25 MNs. This reduction could be accounted for entirely by the 27.4% reduction in the number of α-MNs (WT: 339 ± 17 MNs; TDP-43^{A315T}: 246 ± 9 MNs; **$P = 0.003$). No difference in the total number of γ-MN (ChAT$^+$, NeuN$^-$; <465 μm^2) cells was observed. Error bars represent the 95% confidence interval. (*E*) Distributions of cell body size of all ChAT$^+$ MNs in τ^{ON}hFUS^{WT} animals at P360 (gray bars; 50-μm^2 bins; $n = 4$ animals) and from age-matched τ^{ON}hFUS^{P525L} animals (red bars). Body sizes of ChAT$^+$ MN cells showed a bimodal distribution best fit by two Gaussian curves (correlation = 0.91) representing small (τ^{ON}hFUS^{WT}) (solid gray line), small τ^{ON}hFUS^{P525L} (solid red line), large (τ^{ON}hFUS^{WT}) (dashed gray line), and large τ^{ON}hFUS^{P525L} (dashed red line) populations. These measurements were used to determine the cutoff of the small, ChAT$^+$ γ-MNs. $n = 4$ for all genotypes. Error bars represent the 95% confidence interval. (*F*) Expression of myc-hFUS (red) in the γ-MN population. The γ-MN population was defined by size (<440 μm^2), the presence of ChAT (gray), and the absence of NeuN (green) as indicated by the dotted white lines. (Scale bar: 30 μm.) (*G*) Number of ChAT$^+$ MNs in the L5 segment in τ^{ON}hFUS^{WT} (gray; $n = 4$) and τ^{ON}hFUS^{P525L} (red; $n = 4$) animals. At P360, the large (>440 μm^2) α-MN population is significantly reduced (41%; $P = 0.0001$) in τ^{ON}hFUS^{P525L} animals compared with τ^{ON}hFUS^{WT} animals and WT littermate controls (τ^{ON}hFUS^{WT}: 366 ± 10.2 MNs vs. τ^{ON}hFUS^{P525L} 215 ± 13 MNs). No difference in the total number of γ-MNs (<440 μm^2) was observed (τ^{ON}hFUS^{WT}: 159.7 ± 10.8 MNs vs. τ^{ON}hFUS^{P525L} 160 ± 9 MNs; $P = 0.821$). $n = 4$ for each genotype. **$P < 0.01$ using one-way ANOVA at each time point with Bonferroni's post hoc test. Error bars represent the 95% confidence interval.

mutants demonstrated ~50% reduction of γ-MNs (17), and at end stage in the SOD1^{G93A}/GDNF^{FLOX}/Egr3^{CRE} double mutant the number of the γ-MNs was also reduced by half compared with the SOD1^{G93A}/GDNF^{FLOX} (no Cre) control (73 ± 24 MNs, $n = 4$ vs. 164 ± 12 MNs, $n = 4$; $P = 0.003$) (Fig. 4*G*). Although incomplete, this elimination of γ-MNs resulted in a significant delay

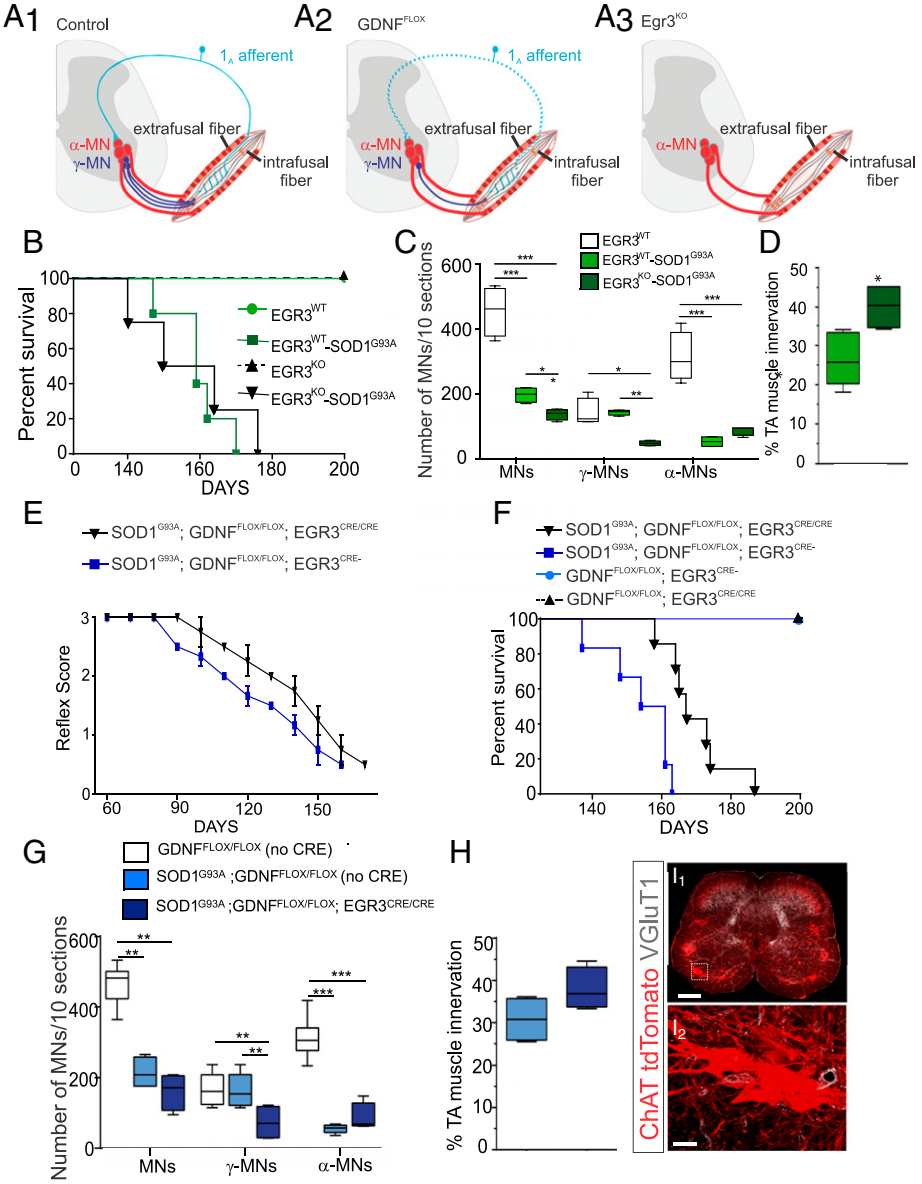

Fig. 4. Loss of sensory inputs increases α-MN survival in SOD1^{G93A} mutant mice. (*A*) Schematic representation of the spinal reflex circuit (A_1). This circuit is perturbed in the GDNF^{FLOX} mice in which reduced γ-MN survival results in a reduction in proprioceptive feedback (A_2). In Egr3^{KO} mice, the circuit is disrupted further, in that degeneration of the muscle spindles results in a deficit in the strength of direct (I_A) sensory-motor connections (A_3). (*B*) Survival analysis of SOD1^{G93A}; Egr3^{KO} double-mutant mice and SOD1^{G93A} mutant controls revealed no significant difference in lifespan (median survival 159 d for Egr3^{WT}; SOD1^{G93A} mice vs. 157 d for Egr3^{KO}; SOD1^{G93A} mice; $P = 0.67$). (*C*) Quantification of the number of ChAT^{+} MNs at end stage (~P157) in SOD1^{G93A}; Egr3^{KO} (138 ± 8; $n = 4$), WT (455 ± 38; $n = 4$; ***$P = 0.001$), and SOD1^{G93A} (198 ± 12; $n = 4$; *$P = 0.01$) animals. As anticipated, a significant decrease in the number of γ-MNs was observed in the Egr3^{KO}; SOD1^{G93A} mice compared with WT and SOD1^{G93A} mutant mice (**$P = 0.01$). In contrast, there was a 10% increase in the number of α-MNs in the double mutant compared with SOD1^{G93A} mice. Error bars represent the 95% confidence interval. (*D*) A significant 14% increase in innervation was observed in the TA muscle of Egr3^{KO}; SOD1^{G93A} animals compared with SOD1^{G93A} animals (*$P = 0.02$). Error bars represent the 95% confidence interval. (*E*) The hind limb reflex score declines earlier in the course of the disease in the SOD1^{G93A}; GDNF$^{FLOX/FLOX}$;Egr3^{NOCRE} animals than in SOD1^{G93A}; GDNF$^{FLOX/FLOX}$; Egr3 $^{CRE/CRE}$ animals from P90 to P140 ($P < 0.05$; two-way ANOVA). (*F*) Lifespan is extended by 10 d in SOD1^{G93A}; GDNF$^{FLOX/FLOX}$; Egr3$^{CRE/CRE}$ animals compared with controls (median survival: 157.5 d in SOD1^{G93A}; GDNF$^{FLOX/FLOX}$; Egr3^{NOCRE} animals vs. 167 d for SOD1^{G93A}; GDNF$^{FLOX/FLOX}$; Egr3$^{CRE/CRE}$ animals; ***$P \leq$ 0.0001). (*G*) Quantification of ChAT^{+} MNs in the L5 segment demonstrates a significant reduction in the total number of MNs in SOD1^{G93A}; GDNF$^{FLOX/FLOX}$; Egr3 CRE/CRE (dark blue) animals when compared with controls [GDNF$^{FLOX/FLOX}$ (no CRE, white); SOD1^{G93A}; GDNF$^{FLOX/FLOX}$ (no CRE, light blue); **$P = 0.0002$]. This difference could be accounted for by the elimination of the γ-MN population in the SOD1^{G93A}; GDNF$^{FLOX/FLOX}$; Egr3$^{CRE/CRE}$ animals (SOD1G93A; GDNFFLOX/FLOX; Egr3^{NOCRE} vs. SOD1^{G93A}; GDNF$^{FLOX/FLOX}$; Egr3$^{CRE/CRE}$: **$P = 0.003$). There was no significant difference in the number of α-MNs in SOD1^{G93A}; GDNF$^{FLOX/FLOX}$; Egr3$^{CRE/CRE}$ when compared with the SOD1^{G93A}; GDNF$^{FLOX/FLOX}$; Egr3^{NOCRE} animals ($P = 0.13$). A decrease in the number of α-MNs is observed in animals carrying the SOD1^{G93A} transgene when compared with WT control animals (***P = 0.0001). Error bars represent 95% confidence interval. (*H*) Quantification of TA muscles showed no significant increase in innervation at disease end stage in SOD1^{G93A}; GDNF$^{FLOX/FLOX}$; Egr3$^{CRE/CRE}$ (dark blue) compared with SOD1^{G93A}; GDNF$^{FLOX/FLOX}$; Egr3^{CRE-} (light blue) animals ($P = 0.10$). Error bars represent the 95% confidence interval. (*I*) MNs in segment L6 visualized in transgenic mice carrying the *tdTomato* reporter (red). Excision of the loxP-flanked STOP cassette by Cre-mediated recombination (ChAT Cre) results in the expression of tdTomato in cholinergic cells. MNs located in Onuf's nucleus (white dotted square shown in higher magnification in I_2) are immunonegative for VGluT1 inputs. As previously described (42), Onuf's nucleus was identified by its characteristic location at the lateral border of the ventral horn. (Scale bars: 250 μm in I_1 and 25 μm in I_2.) Image courtesy of Francisco Alvarez (Emory University School of Medicine, Atlanta, GA).

in the onset of $SOD1^{G93A}$-dependent motor signs as measured by the reduction in the hindlimb extension reflex (40). Loss of the extension reflex first observed at P90 in the $SOD1^{G93A}$ controls was not seen in the $SOD1^{G93A}$; $GDNF^{FLOX}/Egr3^{CRE}$ mutants until P110 (Fig. 4*E*). This delay in the reduction of the extension reflex by ∼15 d ($P < 0.05$, two-way ANOVA) was observed throughout the course of the disease until ∼P150 when the $SOD1^{G93A}/GDNF^{FLOX}$ (no Cre) mice reach end stage (median survival = 157.5 d). In contrast, the $SOD1^{G93A}$;$GDNF^{FLOX}/Egr3^{CRE}$ mutants survive an additional 10 d (mean survival = 167 d; $P < 0.0001$) (Fig. 4*F*), an increase in the median survival comparable to the observed delay in onset. At the delayed end stage, the number of surviving, L4/5 α-MNs in the $SOD1^{G93A}/GDNF^{FLOX}/Egr3^{CRE}$ double mutants (87 ± 21; $n = 4$) was not statistically different from the number at the earlier end stage in the $GDNF^{FLOX}/Egr3^{CRE}$ controls (55 ± 5 MNs; $n = 5$; $P = 0.13$). The same pattern was seen for TA muscle innervation (Fig. 4*H*).

Our analysis of the $GDNF^{FLOX}/Egr3^{CRE}$ mutants revealed that the partial but selective elimination of γ-MNs delays the onset of disease in the $SOD1^{G93A}$ mouse with no apparent effect on progression, resulting in a significant increase in longevity. Reducing muscle afferent activity either by eliminating muscle spindles or by decreasing their sensitivity to stretch by reducing fusimotor inputs mitigates the SOD1 phenotype in terms of α-MN survival and lifespan. These observations demonstrate a pathogenic role of this monosynaptic excitatory input on α-MNs in the pathogenesis of MN disease in this ALS model. The absence of I_A proprioceptive inputs on γ-MNs may account in part for their selective survival in ALS.

Discussion

The selective involvement of specific MN subtypes is a clinical and pathological hallmark of ALS. Here we focus on the γ-MNs, a functionally distinct MN subpopulation that selectively innervates the intrafusal fibers of the muscle spindle. Our data demonstrate that γ-MNs are spared entirely at the end stage of disease in three distinct mouse models of ALS, demonstrating that the resistance of γ-MNs is a common feature of MN disease.

Like other resistant MN populations in ALS, including oculomotor neurons and, as we demonstrate here, MNs of Onuf's nucleus, the γ-MNs lack monosynaptic sensory inputs from the muscle spindle. These observations led us to consider whether this excitatory input might contribute to the selective degeneration of α-MNs in ALS and account in part for the resistance of γ-MNs. Using mouse genetics to manipulate elements of the spinal reflex circuit, we found that reduced proprioceptive feedback on α-MNs improves their survival and that selective elimination of γ-MNs results in a significant delay in disease onset and an increase in the lifespan of $SOD1^{G93A}$ mutant mice. These data are consistent with a model in which afferent activity, and perhaps synaptic excitation generally, accelerates MN degeneration in ALS, suggesting that surviving γ-MNs play a pathogenic role in ALS by increasing muscle afferent firing and thereby hastening disease onset. The effect on MN survival and lifespan that we observe in the SOD1 mouse model as a consequence of functional changes in sensorimotor inputs demonstrates that the relative vulnerability of specific MN subtypes in ALS is determined in part by their connectivity within motor circuits and the functional interactions that control MN activity.

Sparing of γ-MNs in ALS. In this study we use a combination of three molecular markers of γ-MNs—the Hb9::GFP transgene, NeuN, and the GDNF receptor reporter Gfrα1-TLZ—to demonstrate complete and selective sparing of γ-MNs even at late stages of disease in three unrelated transgenic models of ALS respectively expressing mutant $SOD1^{G93A}$, $TDP\text{-}43^{A315T}$, or FUS^{P525L}. Together, these independent markers enable us to identify γ-MN cell bodies in the ventral horn of the spinal cord of these mutants and to address the possibility that the loss of individual markers and changes in MN morphology (29) in the mutant mice may have led to the misidentification of shrunken α-MNs as γ-Ms, a criticism that limited several previous studies suggesting γ-MN sparing in ALS patients and in the SOD1 mouse model (22–26). Moreover, we demonstrate that the majority of NMJs on muscle spindles of the TA muscle remain innervated at end stage, consistent with the complete sparing of γ fusimotor axons that contact ∼90% of intrafusal NMJs (17). The remaining ∼10% of intrafusal NMJs have no associated motor axon, likely as a consequence of the loss of β-skeletofusimotor collaterals of α-MNs (17). Consistent with our findings, one recent study (27) using UCHL1 as a marker of γ-MNs and slow-twitch α-MNs together with the γ-selective marker Err3 (41) supports the idea that γ-MNs are less vulnerable in the $SOD1^{G93A}$ mouse model of ALS. We observe similar sparing of γ-MNs in TDP-43 and FUS transgenic models of ALS, demonstrating that this feature of the disease phenotype is shared by various forms of familial ALS. This shared pattern of selective MN vulnerability in two unrelated models of disease provides further evidence of common pathogenic mechanisms and pathways.

The Role of I_A Afferent Excitation in Motor Neuron Degeneration. The absence of sensory inputs from I_A muscle spindle afferents on γ-MNs, a major source of excitatory stimulation of α-MNs, is one of the features that distinguishes fusimotor from α-MNs. Group I_A afferent inputs are also absent from other ALS-resistant MN populations (Fig. 4*I*), raising the question of whether MN resistance is linked to the absence of sensory input. Gene expression in ALS-resistant MNs is distinct from that of vulnerable MNs (42), and one differentially expressed gene (*sema3e*) is a known repellent for sensory afferent input (43, 44). These findings raise the possibility that molecular distinctions between vulnerable and resistant MNs may influence MN survival in ALS through changes in synaptic connectivity and circuit function.

This idea has been tested in previous studies using sprawling (Swl) and legs at odd angles (Loa) cytoplasmic dynein heavy chain 1 (*Dync1h1*) mutants in which the survival of muscle afferents and other dorsal root ganglion neurons is reduced and the development and maintenance of muscle spindle is affected (45). Loa mice show increased survival compared with SOD1 mutants; however, no increase in survival is seen with the *Swl* mutants (45–47). However, these mutations have multiple effects on axonal transport (45) and mitochondrial function (48), complicating the interpretation of these observations. Here we used a more targeted genetic approach, using the $Egr3^{KO}$ mouse, in which muscle spindle degeneration results in functional loss of I_A proprioceptive afferents (36, 37), to test the idea that I_A excitatory inputs contribute to α-MN degeneration and that their absence could account, at least in part, for the sparing of γ-MNs in the $SOD1^{G93A}$ mouse model of ALS. In the $SOD1^{G93A}/Egr3^{KO}$ double mutant, we did indeed observe a modest (10%) but significant increase in the number of surviving α-MNs in the lumbar spinal cord as compared with the $SOD1^{G93A}$ single mutant, and a more pronounced (∼20%) reduction in the degree of denervation of the most vulnerable TA muscle. These data are consistent with a model in which I_A excitatory inputs contribute to α-MN degeneration in the SOD1 mutant mouse, so that silencing of these inputs improves α-MN survival.

In an excitotoxic model of MN degeneration in ALS, reflex activation of MNs by muscle afferents may contribute to glutamate-dependent and calcium-mediated apoptotic death (49) by increasing MN firing. Early studies of mutant SOD1 mice demonstrated that embryonic MNs are hyperexcitable (50–55), suggesting that a pathological increase in the intrinsic excitability of MNs could lead to excitotoxic MN degeneration (reviewed in ref. 56). However, a recent study shows that the hyperexcitability observed in embryonic mutant SOD1 MNs is transient and that

in the adult SOD1^{G93A} mouse homeostatic mechanisms compensate to restore normal MN excitability (57). In fact, these compensatory mechanisms fail in a substantial subpopulation of hypoexcitable mutant MNs (57). Despite the finding of normal or reduced intrinsic excitability of MNs in the ALS model, excitotoxicity mediated by extrinsic synaptic mechanisms could still lead to excessive excitation and contribute to MN death. Our findings that the MN phenotype improves in the SOD1^{G93A}/Egr3^{KO} and SOD1/GDNF double mutants, in which VGluT1^{+} (58) proprioceptive inputs are silenced, support this model and suggest that primary afferents are one source of excitation contributing to MN degeneration in ALS. However, the benefit we observe is limited, as perhaps not surprising, given that I_A afferents are only one of several sources of excitatory input on MNs. Local interneurons and descending projections also contribute to MN excitation, and elimination of these VGluT2^{+} inputs also has been shown to be protective in the SOD1^{G93A} mouse (59). In ALS, some vulnerable MNs do not receive synaptic input from I_A afferent fibers (60, 61), suggesting that excitotoxicity from I_A afferents alone does not result in MN degeneration. This observation is consistent with our model that excitatory inputs generally contribute to MN degeneration in ALS.

The balance of excitatory and inhibitory drive on MNs in ALS may be altered not only by an increase in excitation but by the loss of inhibitory inputs as well. For example, the recurrent inhibitory circuit mediated by Renshaw cells is altered early in the course of disease in the SOD1^{G93A} mouse by the loss of presynaptic, recurrent motor axon inputs on Renshaw cells, which implies decreased feedback inhibition of MN firing (62). This loss of inhibitory feedback in combination with excess excitatory inputs on MNs—even in the absence of hyperexcitability— could lead to increased firing and the consequent excitotoxic degeneration of MNs in ALS. Consistent with this idea, the ratio of excitatory to inhibitory inputs on α-MNs in the cat is greater in the more vulnerable fast-fatigable MNs that predominate in the TA pool than in the less vulnerable slow MNs (63–65), and, as suggested by Delestrée et al. (57), this may account for the differential sensitivity of these subpopulations in patients and in mouse models of ALS.

Here, we use genetics to silence proprioceptive afferent inputs to MNs early in development by a mechanism independent of mutant SOD1, but previous studies have shown that VGluT1^{+} boutons from proprioceptive afferents on surviving α-MNs are normally lost in the SOD1 mutant (66). This reduction of I_A inputs, which we argue contributes to MN degeneration in the SOD1^{G93A} mouse, may mitigate the SOD1 phenotype as part of a late compensatory mechanism by which the excitatory drive on MNs is reduced in the SOD1-ALS mutant mouse. Indeed, this reduction in excitatory drive may be a general mechanism to reduce the negative effects of MN excitation in the context of MN disease. In mouse models of spinal muscular atrophy (SMA), a similar reduction in muscle afferent inputs on MNs has been observed early in the course of the SMA phenotype (67), before degeneration of hyperexcitable, survival motor neuron (SMN)-deficient MNs. Selective expression of SMN in MNs has been show to rescue several aspects of the SMA phenotype, including abnormalities in excitability and the number of muscle afferent inputs (68).

Selective Elimination of γ-MNs Reveals a Functional Role of Fusimotor Activity in ALS. Interpretation of the Egr3^{KO} data are complicated by the loss in this mutant of several components of the spinal reflex circuit, including the muscle spindle, the I_A afferent, and the γ-MN, making it difficult to attribute the effect on α-MN survival to the loss of excitatory I_A activity or to assess the functional role of γ-MNs in this ALS model. Despite the increased MN survival we observed in the SOD1^{G93A}/Egr3^{KO} double mutant, we did not observe any increase in lifespan. This result is perhaps not surprising, given the modest effect on α-MN number, but another explanation could be that the motor phenotype in these double mutants is complex, in that paralysis caused by mutant SOD1 is superimposed on a sensory ataxia observed in the Egr3^{KO} mutant (36). The sensory ataxia alone has no effect on survival but could exacerbate the motor phenotype of the SOD1^{G93A} mouse and negate any benefit on lifespan gained by improved α-MN survival.

To address these limitations, we analyzed mice in which γ-MNs are selectively eliminated by the conditional knockout of muscle spindle-derived GDNF on which postnatal γ-MN survival depends (17). These GDNF^{FLOX}/Egr3^{CRE} mutants have no overt motor phenotype as a result of γ-MN loss and the consequent decrease in stretch-mediated proprioceptor feedback on α-MNs. Without the complication of muscle spindle degeneration, these mice make it possible to assess the specific role of γ-MN loss and the resulting reduction of proprioceptive feedback on α-MN survival in the SOD1^{G93A} mice. Analysis of these double mutants revealed a significant delay in the onset of motor symptoms and an increase in the average lifespan of the SOD1^{G93A} mice by 12 d, comparable to the benefits seen in this same model of riluzole (69), the only approved therapy for ALS. These data demonstrate that γ-MNs functionally influence the MN phenotype in the SOD1-ALS mouse, hastening the progression to end stage.

Together, our findings of reduced α-MN degeneration in the SOD1/Egr3^{KO} mutant and of γ-MN sparing in all the ALS mutants we have analyzed suggest a model in which fusimotor activity, preserved in ALS, contributes to the SOD1-ALS phenotype by maintaining the sensitivity of muscle spindles to stretch and consequently increasing excitatory feedback on α-MNs in a way that accelerates their degeneration. Fusimotor activity has not been studied directly in the context of ALS, but in other disorders (e.g., stroke) in which descending motor systems are impaired, recent evidence suggests that excess fusimotor drive is associated with spasticity (70), although it is not necessarily causal. Reflex hyperexcitability and spasticity are also a clinical hallmark in ALS, and here, too, γ-MN activity may be one of several mechanisms (71) contributing to the afferent-mediated increase in α-MN firing, leading to their degeneration. In all patients with ALS and especially in those with predominant upper MN findings, limiting fusimotor drive therefore may not only be of symptomatic benefit but also may delay lower MN degeneration and extend the length and quality of their lives.

Experimental Procedures

Transgenic Mice. All animal studies were performed under an approved Institutional Animal Care and Use Committee animal protocol according to the institutional guidelines of the College of Physicians and Surgeons at Columbia University. SOD1^{G93A} [B6.Cg-Tg (SOD1-G93A)1Gur/J] transgenic mice (stock no. 004435; Jackson Laboratory) were genotyped according to the standard PCR protocol. Both male and female SOD1^{G93A} littermates were used in this study, because no significant differences were observed between age- and genotype-matched animals of each sex. Each mouse was considered to have reached the end stage of the disease when it was no longer able to right itself within 15–30 s when laid on either side.

Other mouse lines used in this study include the previously characterized *GDNF$^{FLOX/FLOX}$ Egr3$^{CRE/CRE}$* (17), *Hlxb9-GFP1Tmj* (*Hb9::GFP*; Jackson Laboratory stock no. 005059) (72), and *Egr3^{KO}* (36), kindly provided by Warren Tourtellotte, Feinberg School of Medicine, Northwestern University, Chicago, IL. To label motor neurons in Onuf's nucleus, the tdTomato reporter line (stock no 007909; Jackson Laboratory) was crossed to the ChAT-IRES-Cre deleter strain (stock no. 006410; Jackson Laboratory). As previously described (28), the τhFUS mouse lines were generated using a vector modified from that designed to target the mouse *MAPT* (tau) genomic locus by homologous recombination (73). The τ^{ON} mice were generated by crossing τ^{OFF} and the Protamine-Cre mouse line (stock no. 003328; Jackson Laboratory).

Tissue Collection. Animals were deeply anesthetized using ketamine (100 mg/kg; Ketaset; Pfizer) and xylazine (10 mg/kg; Anased; Lloyd Laboratories) and

were transcardially perfused with 4% (wt/vol) paraformaldehyde in 0.1 M phosphate buffer, pH 7.4 (4% PFA-PB). The spinal cords and TA muscles were dissected and were fixed overnight (spinal cord) or for 3 h (muscles) in 4% PFA-PB. Spinal cords were embedded in 5% (wt/vol) agar and then were cut into 75-μm cross-sections with a Leica vibratome VT 1000S. TA muscles were equilibrated in a gradient of sucrose [10–20–30% (wt/vol)], embedded in optimum cutting temperature (O.C.T.) compound (Sakura), frozen at −20 °C, cut into longitudinal sections (30 μm thick) with a Leica CM 3050S Cryostat, and stored at −20 °C.

Fluorescent Immunohistochemical Analyses. Spinal cord sections were blocked in PBS containing 10% (vol/vol) donkey serum and 0.1% Triton X-100 for 1 h. The sections then were incubated overnight at room temperature in 1% donkey serum and 0.1% Triton X-100 in primary antibody [goat polyclonal anti-ChAT (1:250; Millipore) and mouse monoclonal anti-NeuN (1:1,000; Millipore)]. This step was followed by six 10-min rinses in PBS-0.1% Triton X-100 and incubation for 3 h at room temperature in the corresponding secondary donkey fluorescent antibody (1:500; Jackson ImmunoResearch). The sections were mounted with VECTASHIELD (Vector Labs) after six 10-min washes in PBS.

TA muscle sections were blocked in PBS containing 10% donkey serum and 0.1% Triton X-100 for 30 min. The sections then were incubated overnight at room temperature in 1% donkey serum and 0.1% Triton X-100 in primary antibody [rabbit polyclonal anti-PGP9.5 (1:500; Serotec), α-Bungarotoxin, and Alexa Fluor 647 conjugate (1:1,000)] and for 1 h at room temperature in the corresponding secondary donkey fluorescent antibody (1:1,000; Jackson ImmunoResearch). After washing with PBS-0.1% and Triton X-100, the stained tissue sections were mounted on microscope slides in Fluoromount G (Electron Microscopy Sciences).

Motor Neuron Counts and Size-Distribution Histograms. At each stage, MN counts were performed on the lateral motor column of L4 and L5 spinal segments according to the protocol previously described (17). The histograms represent the average number of MNs in the ventral horn of 10 vibratome sections pooled from the L4/L5 spinal segments of a minimum of three different animals of similar age and genotype. Depending on age, genotype, and section thickness, ∼40–80 MNs were counted per ventral horn. MN size was determined by measuring the cross-sectional area of optical sections in which the MN nucleolus was present; MNs that did not show a regular nuclear shape were excluded from the cell counts. Distribution histograms were constructed by grouping cell-body cross-sectional areas in 50-μm^2 bins. Average histograms were fit to single Gaussian distributions using GraphPad Prism version 5 (GraphPad Software, Inc.). From the fitted distributions we estimated the average cross-sectional area and the SD of the small- and large-sized MN populations. In the histograms, error bars always indicate the SEM. Cell loss was calculated relative to all $ChAT^+$ MNs or relative to the number of cells identified by a particular set of molecular markers or by size criteria. Cutoff sizes for the small and large populations were estimated as the average (expressed in micrometers) + 2 SD (σ) of the respective fitted distribution of small- and large-sized MN populations in control animals.

ACKNOWLEDGMENTS. We thank Francisco Alvarez for comments on the manuscript and for providing images demonstrating the absence of VGluT1 inputs on motor neurons in Onuf's nucleus; Jiejing Chen, Jeffrey Brown, and Margot Elmaleh for expert technical assistance; and Tom Jessell, Chris Henderson, and George Mentis for comments on the manuscript. This work was supported by National Institute of Neurological Disorders and Stroke Grants R01 NS07377 and R21 NS072573 (to N.A.S.), the Columbia University Center for Motor Neuron Biology and Disease, and Target ALS. M.L.-H received a Postdoctoral Research Fellowship Award from the Fond de la Recherche en Santé du Québec.

1. Robberecht W, Philips T (2013) The changing scene of amyotrophic lateral sclerosis. *Nat Rev Neurosci* 14(4):248–264.
2. Carvalho M, Schwartz MS, Swash M (1995) Involvement of the external anal sphincter in amyotrophic lateral sclerosis. *Muscle Nerve* 18(8):848–853.
3. Ferrucci M, et al. (2010) A systematic study of brainstem motor nuclei in a mouse model of ALS, the effects of lithium. *Neurobiol Dis* 37(2):370–383.
4. Iwata M, Hirano A (1978) Sparing of the Onufrowicz nucleus in sacral anterior horn lesions. *Ann Neurol* 4(3):245–249.
5. Kanning KC, Kaplan A, Henderson CE (2010) Motor neuron diversity in development and disease. *Annu Rev Neurosci* 33:409–440.
6. Kubota M, et al. (2000) New ocular movement detector system as a communication tool in ventilator-assisted Werdnig-Hoffmann disease. *Dev Med Child Neurol* 42(1):61–64.
7. Mannen T, Iwata M, Toyokura Y, Nagashima K (1982) The Onuf's nucleus and the external anal sphincter muscles in amyotrophic lateral sclerosis and Shy-Drager syndrome. *Acta Neuropathol* 58(4):255–260.
8. Sung JH, Mastri AR (1980) Spinal autonomic neurons in Werdnig-Hoffmann disease, mannosidosis, and Hurler's syndrome: Distribution of autonomic neurons in the sacral spinal cord. *J Neuropathol Exp Neurol* 39(4):441–451.
9. Dengler R, et al. (1990) Amyotrophic lateral sclerosis: Macro-EMG and twitch forces of single motor units. *Muscle Nerve* 13(6):545–550.
10. Frey D, et al. (2000) Early and selective loss of neuromuscular synapse subtypes with low sprouting competence in motoneuron diseases. *J Neurosci* 20(7): 2534–2542.
11. Saxena S, Caroni P (2011) Selective neuronal vulnerability in neurodegenerative diseases: From stressor thresholds to degeneration. *Neuron* 71(1):35–48.
12. Pun S, Santos AF, Saxena S, Xu L, Caroni P (2006) Selective vulnerability and pruning of phasic motoneuron axons in motoneuron disease alleviated by CNTF. *Nat Neurosci* 9(3):408–419.
13. Spencer RF, Porter JD (1988) Structural organization of the extraocular muscles. *Rev Oculomot Res* 2:33–79.
14. Keller EL, Robinson DA (1971) Absence of a stretch reflex in extraocular muscles of the monkey. *J Neurophysiol* 34(5):908–919.
15. Ellaway PH, Taylor A, Durbaba R (2015) Muscle spindle and fusimotor activity in locomotion. *J Anat* 227(2):157–166.
16. Laporte Y, Emonet-Denand F, Jami L (1981) The skeletofusimotor or beta-innervation of mammalian muscle spindles. *Trends Neurosci* 4:97–99.
17. Shneider NA, Brown MN, Smith CA, Pickel J, Alvarez FJ (2009) Gamma motor neurons express distinct genetic markers at birth and require muscle spindle-derived GDNF for postnatal survival. *Neural Dev* 4:42.
18. Friese A, et al. (2009) Gamma and alpha motor neurons distinguished by expression of transcription factor Err3. *Proc Natl Acad Sci USA* 106(32):13588–13593.
19. Ashrafi S, et al. (2012) Wnt7A identifies embryonic γ-motor neurons and reveals early postnatal dependence of γ-motor neurons on a muscle spindle-derived signal. *J Neurosci* 32(25):8725–8731.
20. Enjin A, et al. (2012) Sensorimotor function is modulated by the serotonin receptor 1d, a novel marker for gamma motor neurons. *Mol Cell Neurosci* 49(3):322–332.
21. Edwards IJ, et al. (2013) Na+/K+ ATPase α1 and α3 isoforms are differentially expressed in α- and γ-motoneurons. *J Neurosci* 33(24):9913–9919.
22. Kawamura Y, et al. (1981) Morphometric comparison of the vulnerability of peripheral motor and sensory neurons in amyotrophic lateral sclerosis. *J Neuropathol Exp Neurol* 40(6):667–675.
23. Sobue G, et al. (1981) Spinal and cranial motor nerve roots in amyotrophic lateral sclerosis and X-linked recessive bulbospinal muscular atrophy: Morphometric and teased-fiber study. *Acta Neuropathol* 55(3):227–235.
24. Conradi S, Ronnevi LO (1993) Selective vulnerability of alpha motor neurons in ALS: Relation to autoantibodies toward acetylcholinesterase (AChE) in ALS patients. *Brain Res Bull* 30(3-4):369–371.
25. Wetts R, Vaughn JE (1996) Differential vulnerability of two subsets of spinal motor neurons in amyotrophic lateral sclerosis. *Exp Neurol* 141(2):248–255.
26. Mohajeri MH, Figlewicz DA, Bohn MC (1998) Selective loss of alpha motoneurons innervating the medial gastrocnemius muscle in a mouse model of amyotrophic lateral sclerosis. *Exp Neurol* 150(2):329–336.
27. Yasvoina MV, et al. (2013) eGFP expression under UCHL1 promoter genetically labels corticospinal motor neurons and a subpopulation of degeneration-resistant spinal motor neurons in an ALS mouse model. *J Neurosci* 33(18):7890–7904.
28. Sharma A, et al. (2016) ALS-associated mutant FUS induces selective motor neuron degeneration through toxic gain of function. *Nat Commun* 7:10465.
29. Kiernan JA, Hudson AJ (1991) Changes in sizes of cortical and lower motor neurons in amyotrophic lateral sclerosis. *Brain* 114(Pt 2):843–853.
30. Gould TW, Yonemura S, Oppenheim RW, Ohmori S, Enomoto H (2008) The neurotrophic effects of glial cell line-derived neurotrophic factor on spinal motoneurons are restricted to fusimotor subtypes. *J Neurosci* 28(9):2131–2146.
31. Wegorzewska I, Baloh RH (2011) TDP-43-based animal models of neurodegeneration: New insights into ALS pathology and pathophysiology. *Neurodegener Dis* 8(4): 262–274.
32. Wegorzewska I, Bell S, Cairns NJ, Miller TM, Baloh RH (2009) TDP-43 mutant transgenic mice develop features of ALS and frontotemporal lobar degeneration. *Proc Natl Acad Sci USA* 106(44):18809–18814.
33. Rao HM, Prevosto V (2013) Proprioceptive eye position signals are still missing a sensory receptor. *J Neurosci* 33(26):10585–10587.
34. Zimmermann L, et al. (2013) Axons giving rise to the palisade endings of feline extraocular muscles display motor features. *J Neurosci* 33(7):2784–2793.
35. Schrøder HD, Reske-Nielsen E (1984) Preservation of the nucleus X-pelvic floor motosystem in amyotrophic lateral sclerosis. *Clin Neuropathol* 3(5):210–216.
36. Tourtellotte WG, Milbrandt J (1998) Sensory ataxia and muscle spindle agenesis in mice lacking the transcription factor Egr3. *Nat Genet* 20(1):87–91.
37. Chen HH, Tourtellotte WG, Frank E (2002) Muscle spindle-derived neurotrophin 3 regulates synaptic connectivity between muscle sensory and motor neurons. *J Neurosci* 22(9):3512–3519.
38. Shneider NA, Mentis GZ, Schustak J, O'Donovan MJ (2009) Functionally reduced sensorimotor connections form with normal specificity despite abnormal muscle spindle development: The role of spindle-derived neurotrophin 3. *J Neurosci* 29(15): 4719–4735.
39. Hunt CC (1990) Mammalian muscle spindle: Peripheral mechanisms. *Physiol Rev* 70(3): 643–663.
40. Urushitani M, et al. (2006) Chromogranin-mediated secretion of mutant superoxide dismutase proteins linked to amyotrophic lateral sclerosis. *Nat Neurosci* 9(1):108–118.

41. Friese A, et al. (2009) Gamma and alpha motor neurons distinguished by expression of transcription factor Err3. *Proc Natl Acad Sci USA* 106(32):13588–13593.
42. Kaplan A, et al. (2014) Neuronal matrix metalloproteinase-9 is a determinant of selective neurodegeneration. *Neuron* 81(2):333–348.
43. Fukuhara K, et al. (2013) Specificity of monosynaptic sensory-motor connections imposed by repellent Sema3E-PlexinD1 signaling. *Cell Reports* 5(3):748–758.
44. Pecho-Vrieseling E, Sigrist M, Yoshida Y, Jessell TM, Arber S (2009) Specificity of sensory-motor connections encoded by Sema3e-Plxnd1 recognition. *Nature* 459(7248):842–846.
45. Chen XJ, et al. (2007) Proprioceptive sensory neuropathy in mice with a mutation in the cytoplasmic Dynein heavy chain 1 gene. *J Neurosci* 27(52):14515–14524.
46. Kieran D, et al. (2005) A mutation in dynein rescues axonal transport defects and extends the life span of ALS mice. *J Cell Biol* 169(4):561–567.
47. Ilieva HS, et al. (2008) Mutant dynein (Loa) triggers proprioceptive axon loss that extends survival only in the SOD1 ALS model with highest motor neuron death. *Proc Natl Acad Sci USA* 105(34):12599–12604.
48. El-Kadi AM, et al. (2010) The legs at odd angles (Loa) mutation in cytoplasmic dynein ameliorates mitochondrial function in SOD1G93A mouse model for motor neuron disease. *J Biol Chem* 285(24):18627–18639.
49. Grosskreutz J, Van Den Bosch L, Keller BU (2010) Calcium dysregulation in amyotrophic lateral sclerosis. *Cell Calcium* 47(2):165–174.
50. Kuo JJ, et al. (2004) Hyperexcitability of cultured spinal motoneurons from presymptomatic ALS mice. *J Neurophysiol* 91(1):571–575.
51. Kuo JJ, Siddique T, Fu R, Heckman CJ (2005) Increased persistent Na(+) current and its effect on excitability in motoneurones cultured from mutant SOD1 mice. *J Physiol* 563(Pt 3):843–854.
52. Meehan CF, Sukiasyan N, Zhang M, Nielsen JB, Hultborn H (2010) Intrinsic properties of mouse lumbar motoneurons revealed by intracellular recording in vivo. *J Neurophysiol* 103(5):2599–2610.
53. Pambo-Pambo A, Durand J, Gueritaud JP (2009) Early excitability changes in lumbar motoneurons of transgenic SOD1G85R and SOD1G(93A-Low) mice. *J Neurophysiol* 102(6):3627–3642.
54. Quinlan KA, Schuster JE, Fu R, Siddique T, Heckman CJ (2011) Altered postnatal maturation of electrical properties in spinal motoneurons in a mouse model of amyotrophic lateral sclerosis. *J Physiol* 589(Pt 9):2245–2260.
55. van Zundert B, et al. (2008) Neonatal neuronal circuitry shows hyperexcitable disturbance in a mouse model of the adult-onset neurodegenerative disease amyotrophic lateral sclerosis. *J Neurosci* 28(43):10864–10874.
56. van Zundert B, Izaurieta P, Fritz E, Alvarez FJ (2012) Early pathogenesis in the adult-onset neurodegenerative disease amyotrophic lateral sclerosis. *J Cell Biochem* 113(11):3301–3312.
57. Delestrée N, et al. (2014) Adult spinal motoneurones are not hyperexcitable in a mouse model of inherited amyotrophic lateral sclerosis. *J Physiol* 592(7):1687–1703.
58. Alvarez FJ, Villalba RM, Zerda R, Schneider SP (2004) Vesicular glutamate transporters in the spinal cord, with special reference to sensory primary afferent synapses. *J Comp Neurol* 472(3):257–280.
59. Wootz H, Enjin A, Wallén-Mackenzie A, Lindholm D, Kullander K (2010) Reduced VGLUT2 expression increases motor neuron viability in Sod1(G93A) mice. *Neurobiol Dis* 37(1):58–66.
60. Faunes M, Oñate-Ponce A, Fernández-Collemann S, Henny P (2016) Excitatory and inhibitory innervation of the mouse orofacial motor nuclei: A stereological study. *J Comp Neurol* 524(4):738–758.
61. Vrieseling E, Arber S (2006) Target-induced transcriptional control of dendritic patterning and connectivity in motor neurons by the ETS gene Pea3. *Cell* 127(7): 1439–1452.
62. Wootz H, et al. (2013) Alterations in the motor neuron-renshaw cell circuit in the Sod1 (G93A) mouse model. *J Comp Neurol* 521(7):1449–1469.
63. Kellerth JO, Conradi S, Berthold CH (1983) Electron-microscopic studies of serially sectioned cat spinal alpha-motoneurons. 5. Motoneurons innervating fast-twitch (type-Ff) units of the gastrocnemius-muscle. *J Comp Neurol* 214(4):451–458.
64. Conradi S, Kellerth JO, Berthold CH, Hammarberg C (1979) Electron microscopic studies of serially sectioned cat spinal alpha-motoneurons. IV. Motoneurons innervating slow-twitch (type S) units of the soleus muscle. *J Comp Neurol* 184(4): 769–782.
65. Brännström T (1993) Quantitative synaptology of functionally different types of cat medial gastrocnemius alpha-motoneurons. *J Comp Neurol* 330(3):439–454.
66. Schütz B (2005) Imbalanced excitatory to inhibitory synaptic input precedes motor neuron degeneration in an animal model of amyotrophic lateral sclerosis. *Neurobiol Dis* 20(1):131–140.
67. Mentis GZ, et al. (2011) Early functional impairment of sensory-motor connectivity in a mouse model of spinal muscular atrophy. *Neuron* 69(3):453–467.
68. Gogliotti RG, et al. (2012) Motor neuron rescue in spinal muscular atrophy mice demonstrates that sensory-motor defects are a consequence, not a cause, of motor neuron dysfunction. *J Neurosci* 32(11):3818–3829.
69. Bellingham MC (2011) A review of the neural mechanisms of action and clinical efficiency of riluzole in treating amyotrophic lateral sclerosis: What have we learned in the last decade? *CNS Neurosci Ther* 17(1):4–31.
70. Mullick AA, Musampa NK, Feldman AG, Levin MF (2013) Stretch reflex spatial threshold measure discriminates between spasticity and rigidity. *Clin Neurophysiol* 124(4):740–751.
71. Roy RR, Edgerton VR (2012) Neurobiological perspective of spasticity as occurs after a spinal cord injury. *Exp Neurol* 235(1):116–122.
72. Wichterle H, Lieberam I, Porter JA, Jessell TM (2002) Directed differentiation of embryonic stem cells into motor neurons. *Cell* 110(3):385–397.
73. Hippenmeyer S, et al. (2002) A role for neuregulin1 signaling in muscle spindle differentiation. *Neuron* 36(6):1035–1049.